Chapter 4 – Experimental methods

The methods used for the evaluation of the electrical parameters of silicon detectors, before and after irradiation, are based on the theoretical development made in Chapter 2. The relevant parameters for the operations of silicon detectors are the full depletion voltage, V_{FD}, the reverse current, I_r and the charge collection efficiency, *CCE*. This chapter describes in detail the experimental methods used in this work and discusses several aspects of these methods that can lead to errors in the evaluation of the electrical parameters under study.

4.1 C-V measurements

The value of V_{FD}, for fixed detector geometry, depends only on the effective doping concentration in the space charge region.

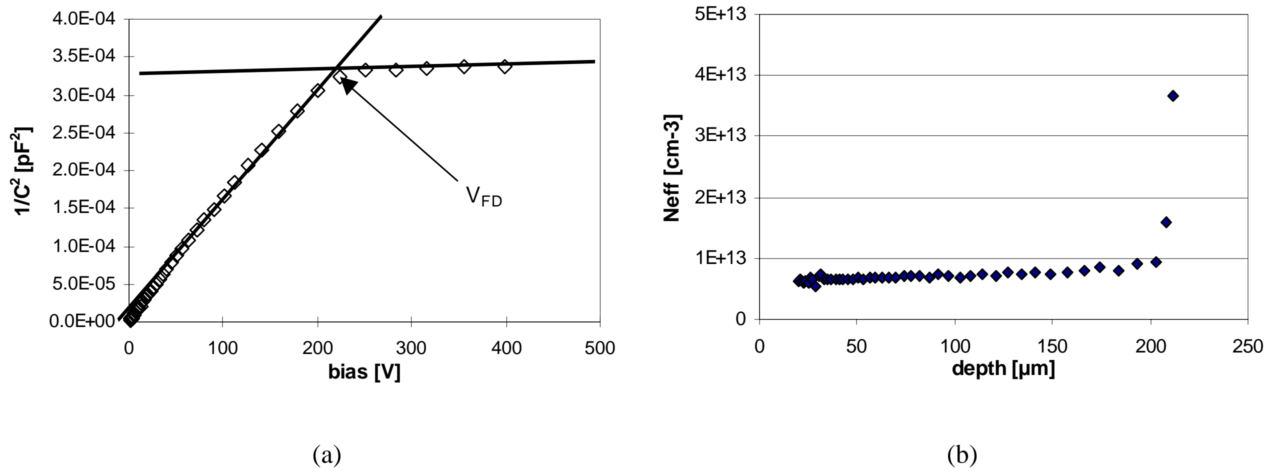

(a) (b)

Fig. 4.1 (a) *$1/C^2$ vs bias for a 200 µm thick non-irradiated diode. N_{eff}, calculated from V_{FD}, is $7.5 \cdot 10^{12}$ cm^{-3}* (b) *N_{eff} profile vs depth. The average value of N_{eff} is in agreement with the value found by the two-line interpolation technique.*

The capacitance voltage measurement allows a simple technique for the V_{FD} evaluation, as described in § 2.2. The crossing point of the two lines obtained by interpolating the slope, in the log-log scale, of the C-V curve below V_{FD} and the constant value of the capacitance above full depletion, provides the estimate of V_{FD}, and then of N_{eff}, according to eq's. 2.31 and 2.32.

Besides, the slope of the C-V curve can also provide the N_{eff} value. The most convenient way to obtain N_{eff} from the slope is the $1/C^2$ versus V plot, shown in Fig. 4.1(a) for a non-irradiated diode. It is apparent that V_{FD} can be easily evaluated with the two-line interpolation technique. N_{eff} determines the slope of the curve. The linearity of the curve below full depletion indicates a homogeneous distribution of the effective doping concentration.

N_{eff} can also be calculated from the C-V slope if its distribution in the diode depth is not homogeneous. In that case the $1/C^2$ characteristic below V_{FD} would not be a straight line. This technique is called differential capacitance method and allows the depth profiling of N_{eff} in an asymmetric abrupt junction [4.1]. This technique is based on the fact that a small increment of the applied reverse bias, dV, induces a current on the diode electrodes. The integral of that current corresponds to the total charge uncovered by the increment, dx, of the depletion region to the detriment of the neutral bulk. The capacitance is given by:

$$C = \frac{1}{dV}\int_0^{\infty} i(t)dt\bigg|_{V_i} = qn(x)A\frac{dx}{dV}\bigg|_{V_i} \tag{4.1}$$

where V_i is the applied reverse bias (below full depletion), $n(x)$ is the free carrier concentration and A is the detector area. The capacitance of a reverse-biased junction, when considered as a parallel plate capacitor, is given by:

$$C = \frac{\varepsilon_{Si} A}{x} \tag{4.2}$$

Differentiating eq. 4.2 and substituting in eq. 4.1, we obtain

$$n(x) = -\frac{C^3}{q\varepsilon_{Si}A^2}\left(\frac{dC}{dV}\right)^{-1} = -\frac{2}{q\varepsilon_{Si}A^2}\left(\frac{d\,{}^{1}\!/\!{}_{C^2}}{dV}\right)^{-1} \tag{4.3}$$

Neglect the minority carrier concentration and supposing a total depletion of majority carriers in the space charge region until the depleted volume edge and a perfect charge neutrality in the neutral bulk beyond that edge (*depletion approximation*), we can assume $N_{eff}(x) \approx n(x)$. The depletion depth, x, is provided by eq. 4.2. The junction approximation is justified for diodes with asymmetric p^+-n or n^+-p junctions and for depth far enough from the junction position [4.1-4.4]. Fig. 4.1(b) shows N_{eff} calculated using this technique for a non-irradiated diode, and the value agrees well with the one found with the two-line interpolation on the C-V or $1/C^2$-V characteristics.

This method could be also applied for the N_{eff} measurement on diodes that cannot be depleted because of a junction breakdown before full depletion. Fig. 4.2 shows an example of C-V measurement for a low resistivity (180 Ω cm) 300 μm thick non irradiated diode for which the breakdown takes place at ≈ 210 volts. In this case, the differential capacitance method allows the estimate of N_{eff}, and of V_{FD} using eq. 2.27. This differential capacitance technique is an efficient method to profile the N_{eff} depth distribution inside the diode and to estimate V_{FD} of detectors for which the full depletion cannot be reached. Unfortunately, this technique cannot be applied to irradiated devices because their C-V characteristics exhibit complex behaviour and the resulting N_{eff} profile is affected by large errors due to the measurement technique of the capacitance.

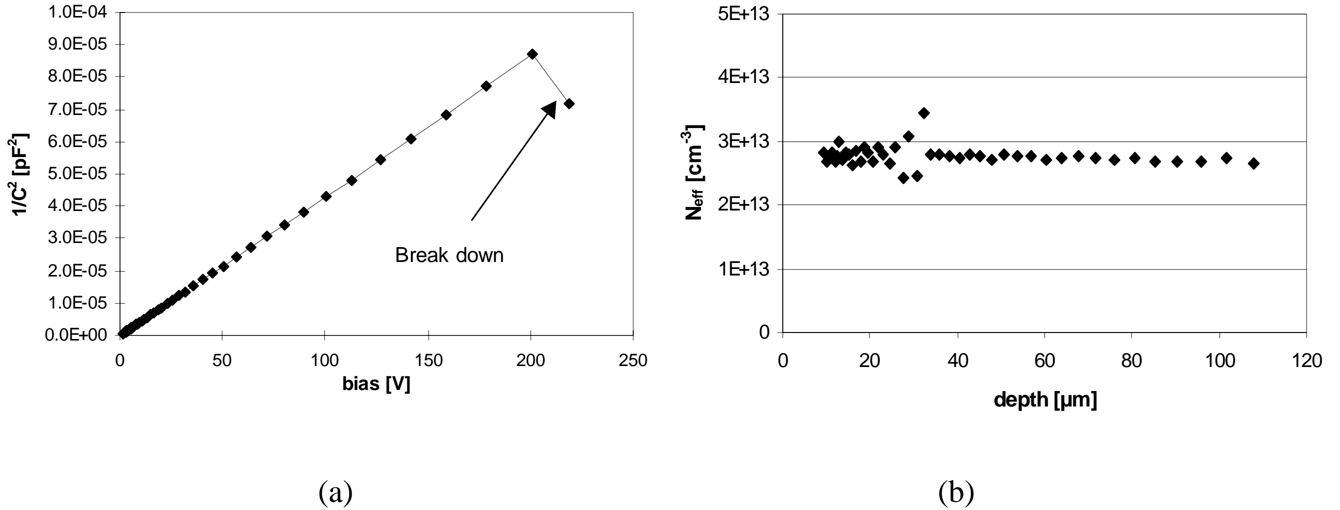

(a) (b)

Fig. 4.2 (a) *$1/C^2$ vs bias for a 300 μm thick non-irradiated low resistivity (180 Ω cm) diode. The detector breakes down before full depletion. (b) N_{eff} profile vs depth. The average value of N_{eff} corresponds to the nominal resistivity. The calculated V_{FD} is ≈ 1900 V.*

The capacitance is evaluated for a given reverse bias, V_I, by superimposing a small oscillating voltage $\Delta V_{AC} = V_{AC}e^{i\omega t}$ and measuring the current variation in the external circuit. The resulting bias applied to the detector is

$$V(t) = V_i + V_{AC}e^{i\omega t} \tag{4.4}$$

where $V_{AC} << V_i$. The current changes are induced by the charge uncovered by the corresponding variation of the depleted bulk depth and swept out by the electric field of the depleted bulk. The variation of the edge of the depleted region is expressed by

$$\Delta x_i(t) = x_i^0 e^{i\omega t} \; . \tag{4.5}$$

Therefore the total number of charges in $\Delta x_i(t)$ is

$$\Delta n(x_i, t) = n(x_i^0) \cdot \Delta x_i(t) \tag{4.6}$$

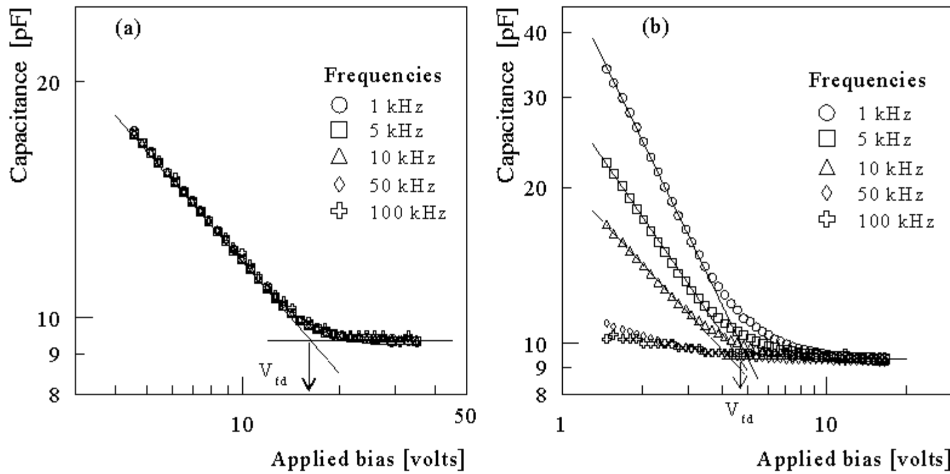

Fig. 4.3 *Typical C-V characteristics with the frequency as a parameter for (a) non-irradiated and (b) irradiated diodes* [4.5].

The C-V characteristics of irradiated detectors exhibit a strong dependence on the frequency of the measuring signal. Figure 4.3 shows the C-V characteristics with the frequency as a parameter for non-irradiated and irradiated diode. The C-V characteristics of the non-irradiated diode exhibit no dependence on the frequency of the measuring signal, while this dependence is apparent for the irradiated one. This dependence is attributed to the deep levels induced by irradiation in the semiconductor bandgap [4.4]. When deep traps are present, the charge variation is due to the shallow doping contribution plus or minus the contribution of the ionised deep levels, depending on the charge state of the levels acting as acceptors or donors. When the deep traps pass from the non-depleted bulk in thermal equilibrium to the depleted region of the detector, because of the variation of the bias voltage induced by the measuring signal, their charge state variations are regulated by carrier emissions or capture processes. The time $\tau_{e,c}$ associated with these processes is defined by:

$$\tau_{e,c} = \frac{1}{g_{e,c}} \tag{4.7}$$

where $g_{e,c}$ is the emission (e) or capture (c) rate. The limiting process is usually the emission rate ($g_e < g_c$), therefore the traps contribute to the capacitance measurement only if the emission rate can follow the measuring signal, so if $g_e > \omega$. On the other hand, if $g_e < \omega$ the measured capacitance depends on the frequency. The frequency dependence of a deep level, which density in the silicon bulk is N_T, can be expressed as it follows [4.6]

$$N_T(\omega) = \frac{N_T}{1+\omega^2 \tau_e^{\,2}} \tag{4.8}$$

The quantity of interest for N_{eff} measurement is the steady state value N_T ($\omega = 0$). Therefore the evaluation based on the differential capacitance technique does not supply the correct value. Also the evaluation of the depth co-ordinate, x, using eq. 4.2 is affected by error. In fact the calculation of the capacitance of the depleting diode as a parallel plate capacitor cannot be applied when the capacitance depends also on the frequency and not only on the diode geometry. The possible correction to find N_T by mean of eq. 4.8 can be applied in the case of one deep level contributing to N_{eff}. Microscopic analyses have shown a composite structure of the radiation-induced levels in the silicon bandgap.

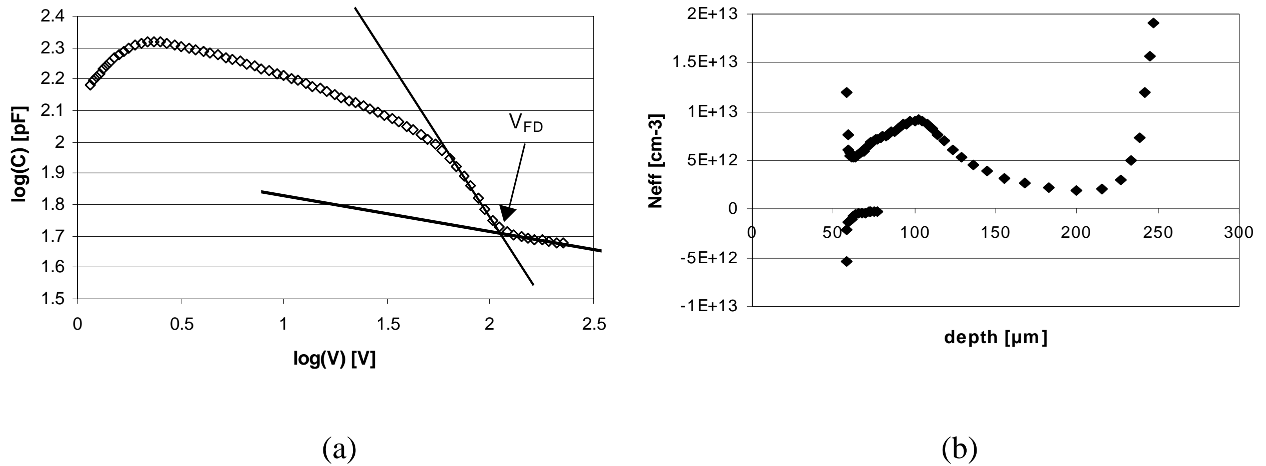

(a) (b)

Fig. 4.4 (a) *C-V characteristic of an irradiated type-inverted diode.* (b) N_{eff} *profile versus depth.*

A singular behaviour of the C-V measurement in irradiated diodes is found at high frequency (> 50^4 Hz) of the measuring signal: the diode capacitance assumes the value of the detector geometrical capacitance (eq. 4.2 with $x = w$, where w is the detector thickness) irrespectively to

the bias voltage (Fig 4.3). This means that no charge carriers are able to follow the fast measuring signal ($N_T \approx 0$ in eq. 4.8) and thus no free carriers are available for the conduction at the edge of the non-depleted region. The carriers are trapped at the defect levels in the non-depleted bulk and their emission rates are not fast enough to follow the measuring signal. Therefore, the non-depleted neutral bulk has very few free carriers and behaves as an insulator, at least for the high-frequency signals and it is *transparent* to the capacitance measurement. The measuring signal penetrates the non-depleted bulk and the free charge located at the electrical contact of the detector can follow the signal. The result of the measurement corresponds to the geometrical capacitance of the diode.

Moreover, the C-V characteristics of irradiated silicon detectors show a non-linear trend before full depletion. In inverted diodes the C-V characteristics show even a rise at low reverse bias voltages (Fig. 4.4(a)). These behaviours cannot be explained by the deep trap presence and there are no special reasons to believe an inhomogeneous depth distribution of radiation induced defects, that can follow the profile shown in Fig. 4.4(b). Furthermore, the behaviour of the CC in irradiated detectors (see Chapter 6) indicates that the depletion volume is still proportional to $V^{1/2}$, implying the homogeneity of N_{eff} in the detector bulk. Therefore, the profiling method does not provide the actual distribution of N_{eff} and cannot be applied to irradiated silicon detector. The assumption of the silicon diode acting as a simple parallel plate capacitor in the depletion approximation seems to be inadequate to describe the C-V characteristic of irradiated devices. Chapter 6 will present a model to interpret the diode changes as a function of the fluence.

Coming back to the problem of V_{FD} (or N_{eff}) evaluation in irradiated devices from the C-V characteristic, it is possible to observe (Fig. 4.4(a)) that the two-line intersection point technique is still applicable to estimate V_{FD}. The frequency used for the C-V measurement was 10 kHz. The error bars for the estimate have been established for any C-V curve, taking into account the possible different *reasonable* choice of points for the two-lines fitting. The systematic error in the voltage measurement has been estimated to be ≈ 1%, which is negligible compared to the error made in the analysis of the C-V curve.

Checks of the reliability of the V_{FD} estimate have been done evaluating V_{FD} by charge collection techniques, as described in § 4.3.

4.2 I-V measurement

The correlation between the leakage current and the radiation damage is based on the assumption that the measured current is dominated by the bulk generation current and then it is proportional to the density of radiation induced defects and to the depleted volume. The measurement is performed at full depletion, when the total bulk of the detector contributes to the reverse current.

The value of the reverse current at full depletion is divided by the detector volume, to give the current per unit of volume (I_{vol}), which can be compared to the radiation induced defect density. The current data are normalised to room temperature using eq. 3.10.

Errors in the measurement of I_{vol} can arise from errors in the evaluation of V_{FD}, of the depleted volume and from sources of leakage current other than the generation current in the detector bulk.

If the guard-ring (G-R) is biased to the same voltage as the central contact, the diode volume is well defined and the lateral extension of the depleted volume is limited to ≈ 1% (§ 2.4.1). The current generated in the bulk underneath the G-R area and the extra-current from the diode edges are collected through the G-R. The current flowing in the central contact is reasonably free of these extra contributions and corresponds to the volume bulk current.

When the G-R is left floating, the extension of the depletion volume towards the diode edge involves a volume larger than the diode volume (the volume defined by the surface of the contact and the depth of the depleted region). It is possible to make a first order correction for the extension of the diode volume, calculating the effective area of the depleted volume from the C-V measurement (eq. 2.26) and using a truncated pyramid approximation of the depleted volume (the upper surface is defined by the junction area). More important, the current flowing through the detector edges is measured by the central contact. In that case, the current measured is larger than the volume generated current. The difference can be very important, especially for highly irradiated diodes and the current can not be correlated to the concentration of radiation induced defects.

Figure 4.5 shows the I-V characteristic of diode irradiated to different fluences and measured with and without connecting the G-R. The G-R current can be calculated from the difference

between the two curves. It is apparent that it does not saturate at full depletion and exhibits an almost ohmic behaviour. The current flowing through the biased G-R is due to the generation current in the depleted volume beneath the G-R and to extra current contributions, as discussed in § 2.4.1. The fact that the G-R current does not saturate shows that extra currents are dominant.

Fluence **[cm^{-2}]**	**V_{fd}** **[V]**	**I_r total (no G-R)** **[µA cm^{-3}]**	**I_r bulk (G-R)** **[µA cm^{-3}]**	**G-R bulk component** **[µA cm^{-3}]**	**G-R extra current** **[µA cm^{-3}]**
0	115	3.6	1.9	0.3	1.4
$2.55 \cdot 10^{12}$	101	45	39	5.6	0
$5 \cdot 10^{12}$	92	90	78	11.1	0.8
$9.6 \cdot 10^{12}$	79	158	137	19.6	1.3
$2.7 \cdot 10^{13}$	42	485	421	60	4
$5.2 \cdot 10^{13}$	21	1035	838	120	77
$7.5 \cdot 10^{13}$	33	1489	1153	165	171
$1.1 \cdot 10^{14}$	78	2753	1769	253	731
$1.7 \cdot 10^{14}$	12	4304	2495	356	1452
$2.2 \cdot 10^{14}$	225	6678	4827	690	1161

Table 4.1 *Different components of the reverse current. The 3rd and 4th column are obtained from measurements with and without the G-R. The sum of the 5th and 6th columns gives the total G-R current.*

The contribution of the generation component can be estimated using the volume bulk current multiplied by the volume underneath the G-R. Table 4.1 shows the total and bulk currents measured without and with G-R, respectively and the bulk and extra-bulk components of the G-R current for detectors irradiated at various fluences with 24 GeV/c protons. It can be observed that the extra-bulk current becomes important after a fluence $\approx 3 \cdot 10^{13}$ cm^{-2}.

Figure 4.6 shows ΔI_{vol} as a function of the fluence measured with and without contacting the G-R. The curves are linear and similar up to $\approx 3 \cdot 10^{13}$ cm^{-2}. Before that fluence the G-R current is

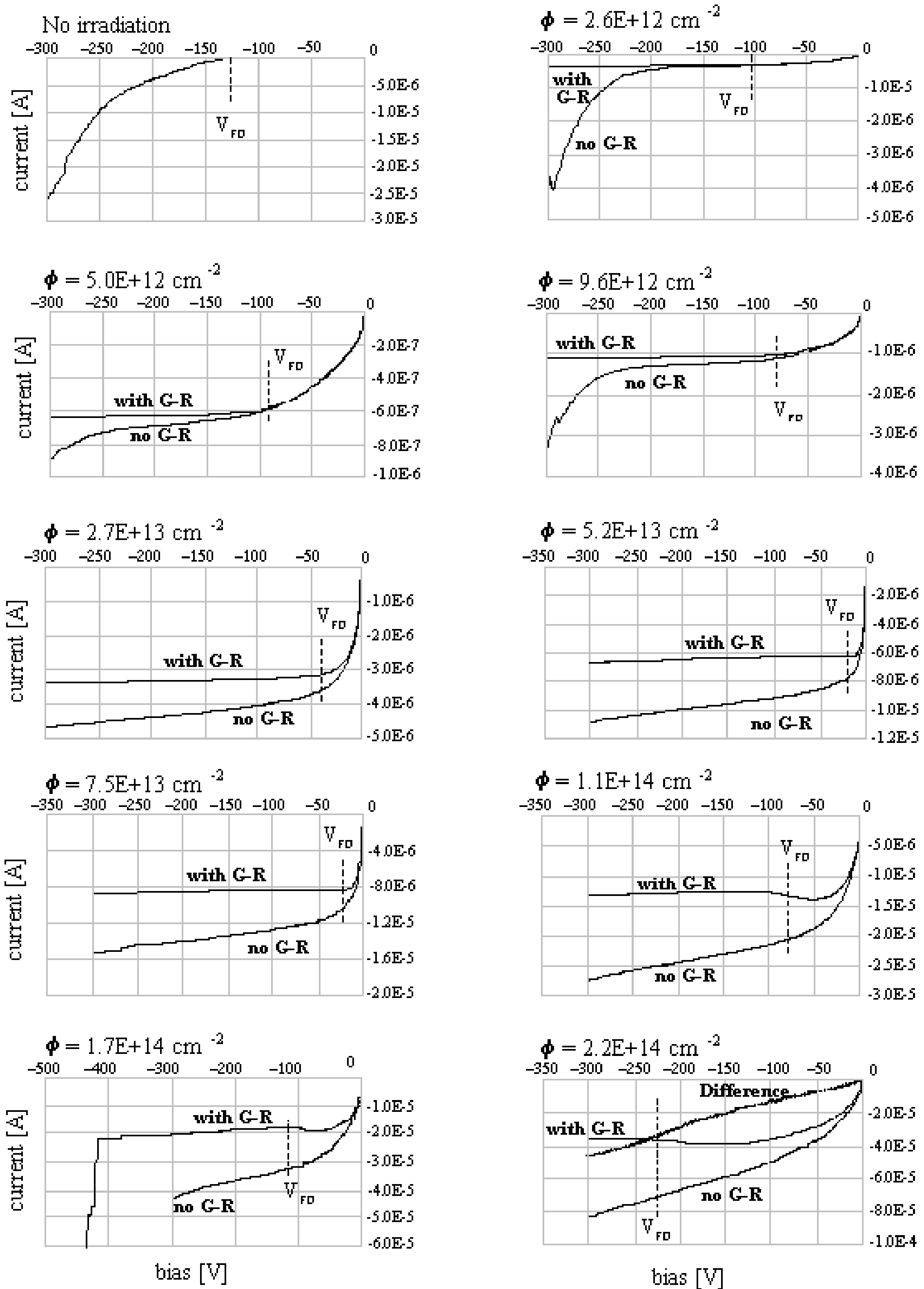

Fig. 4.5 *Leakage current as a function of the reverse bias for variously irradiated silicon diodes with floating and biased guard ring. The reverse current for the non irradiated diode is the same with and without G-R.*

due to the bulk component. The first order correction, applied by evaluating the extension of the depleted volume on the basis of the C-V measurement, is efficient and the two curves are practically superimposed. Increasing the fluence, the extra-bulk contribution becomes more and more important and the current measured without G-R starts to diverge from linearity. At the highest fluences, the current measured without G-R can be larger than the bulk current for a factor of two. For practical reason, most of the measurements of the leakage current have been performed with floating G-R. Therefore, the calculation of the radiation damage constant for the current, α, has been performed limiting the fit to the lowest fluences.

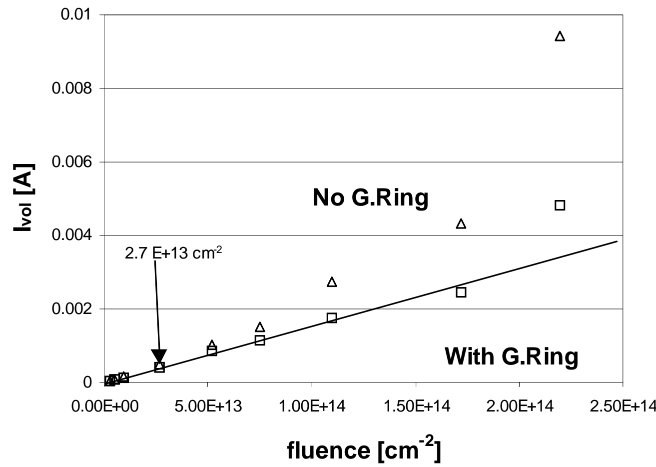

Fig. 4.6 *The volume reverse current as a function of fluence measured with and without bias on the G-R.*

4.3 Charge Collection measurements

Signal formation in silicon detectors

Figure 4.7 shows a reverse biased p^+-n junction. The applied reverse bias is larger than V_{FD} and the diode is overdepleted. The expression of the electric field inside the depleted bulk is:

$$E(x) = -\frac{qN_{eff}}{\varepsilon_{Si}}(x-w) + \frac{V-V_{fd}}{w} = -ax+b \tag{4.9}$$

The electric field lines are normal to the diode surface and are directed from the anode (n^+ ohmic contact) towards the cathode (p^+ contact). The constant b expresses the maximum value of electric field at the junction, and $E_{min} = (-aw + b)$ is the minimum value of the electric field

at the n^+ contact. When an ionising particle passes through the detector, electron-hole (e-h) pairs are created along the path of the particle track. They are separated, before they can recombine, by the electric field in the depleted bulk and drift towards the anode (electrons) or the cathode (holes).

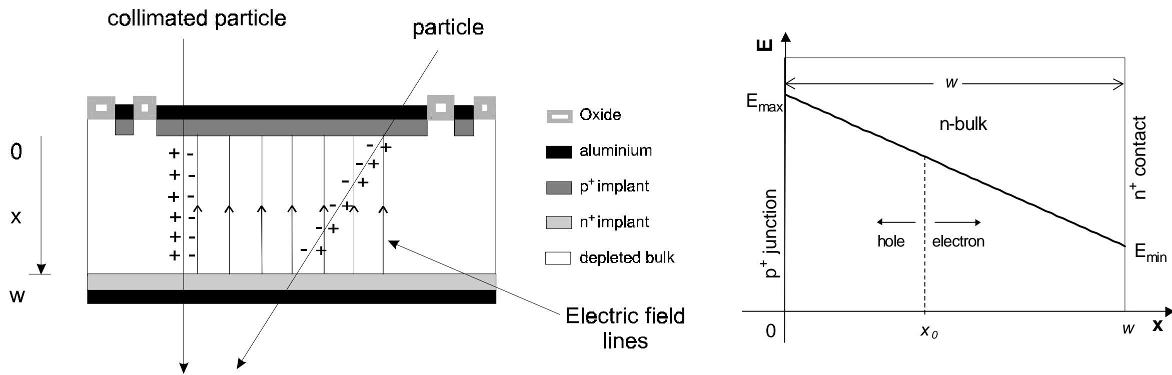

Fig. 4.7 *Generation of carriers along the path of particle tracks and electric field distribution in the silicon diode.*

The movement of the generated charge induces a signal on the detector electrodes according to Ramo's theorem [2.7]

$$\Delta Q = Q\frac{\Delta x}{w} \tag{4.10}$$

where w is the detector thickness. The induced current is given by:

$$i(x) = \frac{dQ}{dt} = \frac{Q}{w}\frac{dx}{dt} = \frac{Q}{w}\mu E(x)\,. \tag{4.11}$$

The drift velocity of electrons and holes can be expressed as it follows:

$$\frac{dx_e}{dt} = -\mu_e(ax-b) \tag{4.12a}$$

$$\frac{dx_h}{dt} = \mu_h(ax-b) \tag{4.12b}$$

where $\mu_{e,h}$ is the mobility of electrons or holes. The integration of eq. 4.12 for a unit charge generated at $x = x_0$ gives, for electrons and holes, respectively:

$$x_e(t) = \frac{b}{a} + (x_0 - \frac{b}{a})\exp(-\mu_e at) \tag{4.13a}$$

$$x_h(t) = \frac{b}{a} + (x_0 - \frac{b}{a})\exp(\mu_h at) \tag{4.13b}$$

The velocity is then:

$$v_e(t) = -\mu_e(ax_0 - b)\exp(-\mu_e at) \quad (4.14a)$$

$$v_h(t) = \mu_h(ax_0 - b)\exp(\mu_h at). \quad (4.14b)$$

We can define the collection time T_{ce} for electrons and T_{ch} for holes as it follows:

$$T_{ce} = \frac{1}{a\mu_e}\ln\left(\frac{ax_0 - b}{aw - b}\right), \quad x(T_{ce}) = w \quad (4.15a)$$

$$T_{ch} = \frac{1}{a\mu_h}\ln\left(\frac{b}{b - ax_0}\right), \quad x(T_{ch}) = 0 \quad (4.15b)$$

The current induced by electrons and holes as a function of time is given by:

$$i_e(t) = \frac{q\mu_e}{w}(ax_0 - b)\exp(-\mu_e at), \qquad 0 \le t \le T_{ce} \quad (4.16a)$$

$$i_h(t) = \frac{q\mu_h}{w}(ax_0 - b)\exp(\mu_h at), \qquad 0 \le t \le T_{ch}. \quad (4.16b)$$

The signal due to holes increases with time and the signal due to electrons decreases with time. The charge collected is evaluated by the integration over time of the hole and electron currents:

$$Q_e(t) = \frac{-q}{aw}(ax_0 - b)[\exp(-\mu_e at) - 1] \qquad 0 \le t \le T_{ce} \quad (4.17a)$$

$$Q_h(t) = \frac{q}{aw}(ax_0 - b)[\exp(\mu_e at) - 1] \qquad 0 \le t \le T_{ch} \quad (4.17b)$$

$$Q_{etot} = \frac{q}{w}(w - x_0) \quad (4.18a)$$

$$Q_{htot} = \frac{q}{w}x_0 \quad (4.18b)$$

The sum of both contributions gives the unit charge injected.

The total current is the convolution of the currents produced by all the generated charges:

$$i_{Te}(t) = \frac{\mu_e}{w}\int_0^w Q(x')(ax' - b)\exp(-\mu_e at)dx' \quad (4.19a)$$

$$i_{Th}(t) = \frac{\mu_h}{w}\int_0^w Q(ax' - b)\exp(\mu_h at)dx' \quad (4.19b)$$

where *Q(x)* is the distribution of the generated charge along the detector depth. The observable signal is obtained by the response of the amplifying chain

$$V(t) = GR_A\int_{-\infty}^{+\infty} i_T(t)dt \quad (4.20)$$

where $i_T(t)=i_{Te}(t) + i_{Th}(t)$, G and R_A are the gain and the resistance (50Ω) of the amplifying network, respectively.

The charge distribution depends on the energy loss of the ionising particle in the detector bulk. A particular case is whether the charge is created in a very shallow layer of the detector, so that the depth distribution can be neglected. We can consider the charge created at $x_0 = 0$ for front (junction side) injection and $x_0 = w$ for rear (ohmic side) injection. When the ionisation takes place next to the junction of an n-type diode, the contribution of holes to the signal is negligible (eq. 4.18(a) with $x_0 = 0$). Only the electron motion induces the signal, so this situation is called electron injection. The opposite is found when the ionisation is distributed in a shallow layer next to the ohmic contact, and it is called hole injection. Figure 4.8(a) shows the ideal shape of the electron signal as a function of the time after the ionisation at two different biases such that $V_{FD} < V_1 < V_2$. The electrons move from the high field region at $x_0 = 0$ towards the anode in the direction of the decreasing electric field. The maximum current is at the beginning of the motion. Therefore the maximum height of the pulse takes place at the injection time and it does not change by increasing the bias. We will call *peaking time* (t_p) the time corresponding to the maximum of the current pulse. The total length of the pulse depends on the strength of the electric field. Higher electric fields allow faster collection because of the increase of the carrier velocity, until the saturation of the drift velocity [2.1]. The collection time of electron with $V > V_{FD}$ is

$$T_{ce} = \frac{1}{a\mu_e} \ln\left(\frac{b}{b - aw} \right) \tag{4.21}$$

T_{ce} decreases while b increases, where b is the maximum value of the electric field at the junction.

Figure 4.8(b) shows the ideal current pulse shape for shallow injection through the rear side ($x_0 = w$) of a fully depleted detector. The charge collection starts when the reverse bias is $V \geq V_{FD}$. The signal is due to holes moving from the region of the lowest to the region with the highest strength of the electric field. The peaking time corresponds to the arrival of carriers in the highest field next to the junction, at the end of their motion. In this case t_p coincides with the collection time of holes and it changes as a function of the reverse bias. T_{ch}, or t_p, decreases while the applied reverse bias increases, according to:

$$T_{ch} = \frac{1}{a\mu_h} \ln\left(\frac{b}{b - aw} \right) \quad (4.22)$$

The analysis of the pulse shape induced by shallow ionisation provides useful information about the electric field distribution in the detector.

The charge collection studies in the present work have been performed using α and β particles from radioactive sources, low energy protons from a Van der Graaf accelerator and red light from a LED diode.

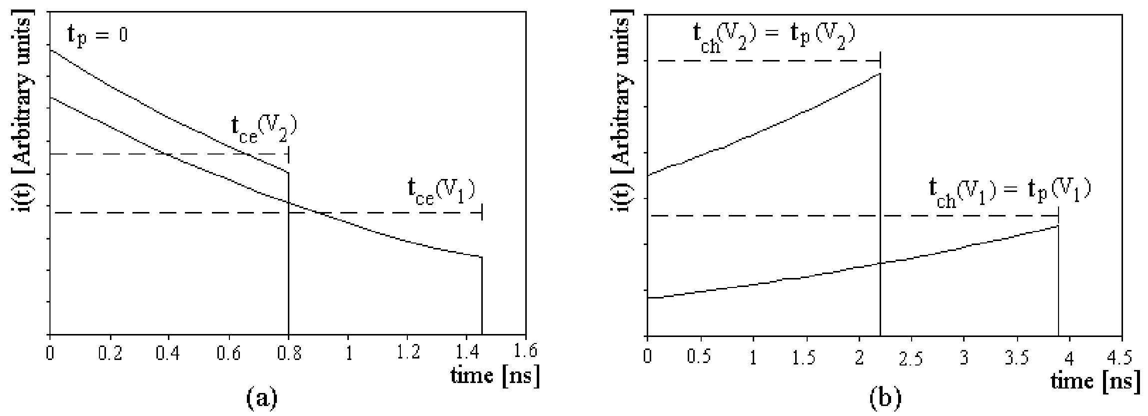

Fig. 4.8 *Ideal pulse shape for (a) electron injection (junction side) and (b) hole injection (ohmic side) of an n-type silicon detector.* $V_{FD} \geq V_1 \geq V_2$.

4.3.1 β particles

A ^{106}Ru source emits β particles (electrons) with energies up to ≈ 3 MeV. A collimator was used to select the particles whose direction is perpendicular to the detector surface (see Fig 4.7) and a scintillator associated with an absorber (see Appendix A) was used to select electrons with energy ≥ 2 MeV which are, to a good approximation, minimum ionising particles (MIPs) in silicon.

A MIP particle traverses a 300 μm thick silicon detector and the charge is uniformly distributed along its path in the detector. The energy deposited by MIPs in semiconductor detectors follows the Landau distribution [4.7]. The most probable energy loss in a 300 μm thick silicon detector is 78 keV ± 10%. The average energy required to create an e-h pair in silicon is 3.6 eV and therefore MIPs create, in 300 μm silicon detectors, about 22000 e-h pairs,

with an ionisation rate ≈ 260 eV/µm [4.8]. In under-depleted detectors only the charge deposited in the active volume is collected by the diode electric field. Therefore, the charge collection for β illumination is proportional to depth of the depleted bulk, or to $V^{1/2}$, until the maximum value corresponding to the full depletion of the detector.

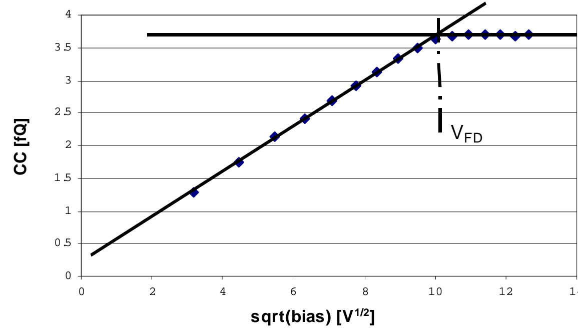

Fig. 4.9 *CC curve as a function of the square root of bias in the case of β particle Illumination.*

The charge collection, *CC*, can be expressed by:

$$CC = x \cdot \rho = D \cdot \sqrt{V} \cdot \rho, \qquad V < V_{FD} \tag{4.23}$$

$$CC = Q_0, \qquad V \geq V_{FD}$$

where the constant *D* is calculated from eq. 2.27, ρ is the deposited charge rate per unit of length and Q_0 is the total collected charge. Q_0 is calculated from the integral of the voltage signal (S) using:

$$Q = \frac{\int S dt}{R_{in} G} \tag{4.24}$$

where R_{in} is the input impedance and G is the gain of the fast current amplifier. Figure 4.9 shows the charge collection curve for a 300 µm thick diode as a function of $V^{1/2}$. The maximum charge collected is ≈ 3.7 fC corresponding to about 23000 electrons, close to the expected value. The intersection point of the two trend-lines, before and after V_{FD}, provides the estimate of V_{FD}.

The CC curve is drawn taking the most probable value of the energy loss distribution at each bias, as results from the Landau fit of the corresponding spectrum (Fig. 4.10). This procedure is quite long, because of the high statistic needed for each energy spectrum (≥ 6000 triggers).

Another method to obtain the CC curve is the average of the deposited charge. The average value of the energy distribution is ≈ 20% larger than the most probable value.

Figure 4.11 shows the β induced pulse shape in a depleted detector resulting from the average of ≈ 1000 triggers and the integral of the signal. The average charge collected from the detector is calculated using equation 4.22. The average method has been used for most practical purposes, because it is faster than the method that uses the most probable value of the Landau distribution.

Appendix A describes the experimental set ups used for the charge collection measurements.

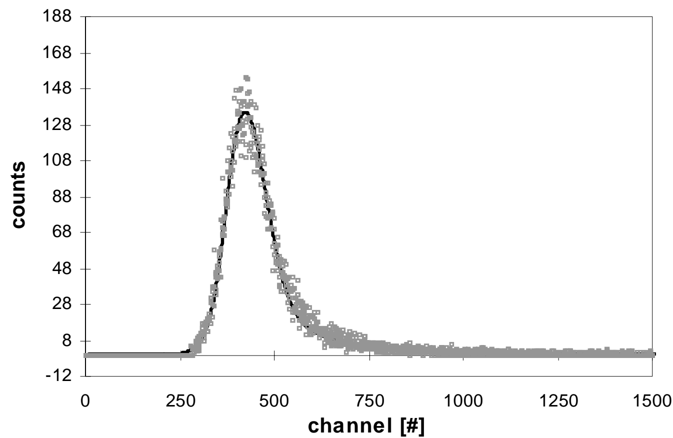

Fig. 4.10 *Landau distribution of the energy loss of a MIP in a 300 µm thick silicon detector. The most probable value is ≈ 80 keV.*

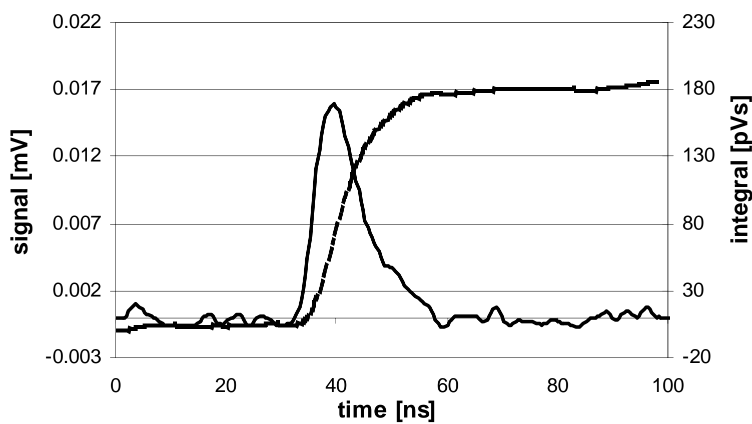

Fig. 4.11 *Averaged signal pulse shape and integral of the signal induced by β particles in A 307 µm thick silicon detector.*

4.3.2 Low range particles: α particle and low energy protons

The energy of protons and α particles necessary to pass through 300 μm of silicon is ≈ 6 MeV and 23 MeV respectively [4.9]. For lower energies, these particles stop into the detector bulk, loosing all their energy inside the silicon detector. The energy deposition follows the Bragg's curve [4.8], the maximum of which is at the end of the particle range (the Bragg's peak). Figure 4.12 shows the energy deposition of 1.7 MeV protons as a function of the depth into silicon detectors simulated using the TRIM package [4.10].

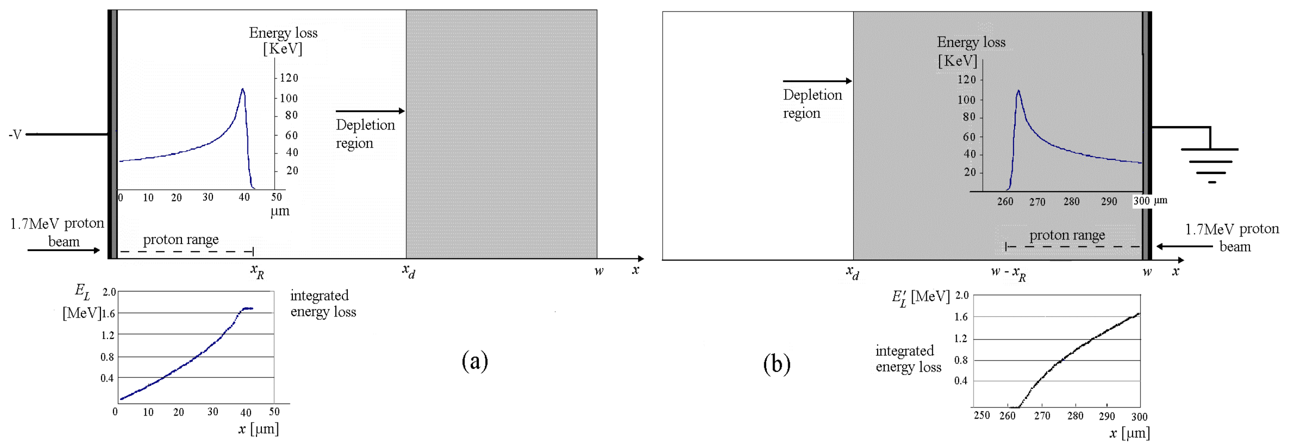

Fig. 4.12 *Energy loss of 1.7 MeV protons in silicon as a function of the path (Bragg's curve) and integrated energy loss as a function of the depletion depth in case of (a) front injection and (b) rear injection.*

If the particles are injected through the junction side of a non-irradiated detector, the charge deposited in the depleted part of the detector is collected. The charge carriers generated in the neutral non-depleted bulk recombine fast in absence of an electric field and no signal is visible on the diode electrodes. Whether the depleted depth, x_d, is larger than the particle range, x_R, the charge created by the ionising particles is entirely collected. Figure 4.10(a) shows the energy loss, as a function of the depletion depth, of low range particles that illuminate the junction side of a silicon detector. The CC can be expressed by:

$$CC = \int_0^x \rho(x')dx' = \frac{1}{3.6} qE_L(x) = Q(x), \qquad V < V_R \qquad (4.25a)$$

$$CC = Q_o, \qquad V \geq V_R \qquad (4.25b)$$

where V_R is the reverse bias voltage corresponding to a depletion depth equal to the particle range, $\rho(x)$ is the density of the deposited charge as a function of the depth, E_L is the energy deposited along the range x and $Q_0$is the total created charge.

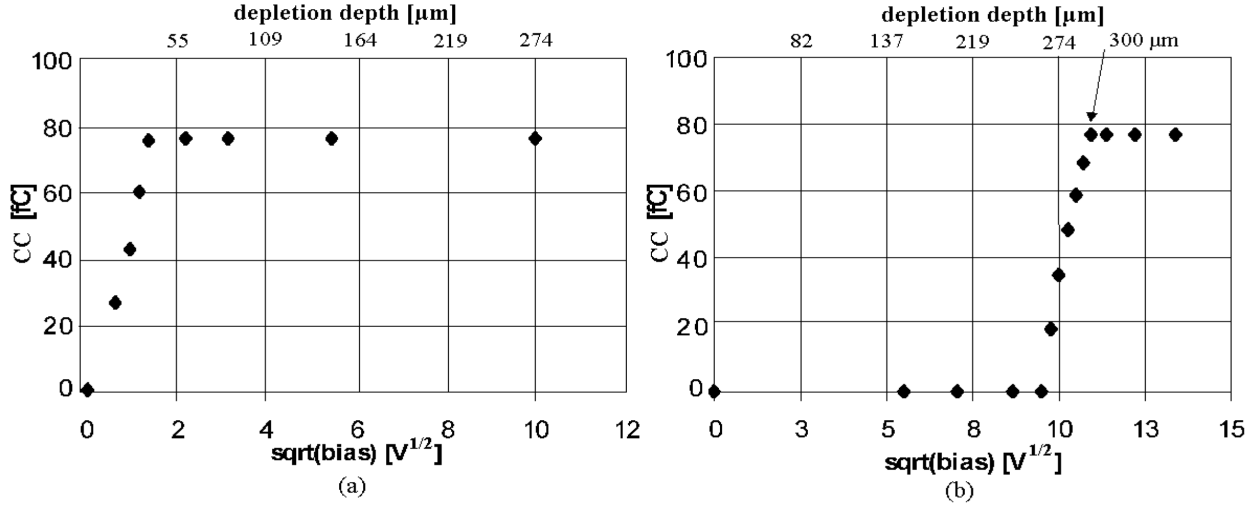

Fig. 4.13 *Simulated charge collection for front (a) and rear (b) illumination with 1.7 MeV protons in a silicon detector with* V_{FD} *= 120 volts.*

Whether the charge is injected from the rear side, the energy is released in non-sensitive region until the depleted volume does not reach the ionisation depth. The CC can be expressed as:

$$CC = 0\,, \qquad V < V'_R \qquad (4.26a)$$

$$CC = Q'(x) = \int_{w-x_R}^{x_d} \rho'(x')dx' = \frac{1}{3.6} qE'_L(x)\,, \qquad V'_R \leq V < V_{FD} \qquad (4.26b)$$

$$CC = Q_o\,, \qquad V \geq V_{FD} \qquad (4.26c)$$

where V'_R is the bias voltage required to deplete the detector up to the depth w-x_R. Figure 4.13 shows a simulation of the ideal charge collection in a detector that depletes at 120 volts, for front or rear side illumination. In the case of front injection, the complete charge collection takes place when the depleted region overcome the particle range. In the case of rear illumination, the charge collection starts when the depletion region reaches the ionisation depth, w-x_R, and achieves the maximum value at full depletion. The electron and hole contributions to the collected charge are not equal, as is the case of β illumination. The e-h pairs are not homogeneously distributed along the detector, but the ionisation is limited to the

depth of the particle range, x_R. When particles are injected through the front side, the path of the electron of a pair generated at $x = x_0$ is $d_e = w - x_0$ to reach the anode, and the path of the hole is $d_h = x_0$ to reach the cathode. For low range particle d_h is always much less than d_e, therefore the contribution to the collected charge is larger for electrons than for holes (eq. 4.18). The opposite is found when the particles illuminate the rear side and d_e is much less than d_h. The CC curves of low range particles are obtained evaluating the centre of the gaussian distribution of the energy loss spectrum (Fig. 4.14(a)) or calculating the integral of the average of the signal (Fig. 4.14(b)).

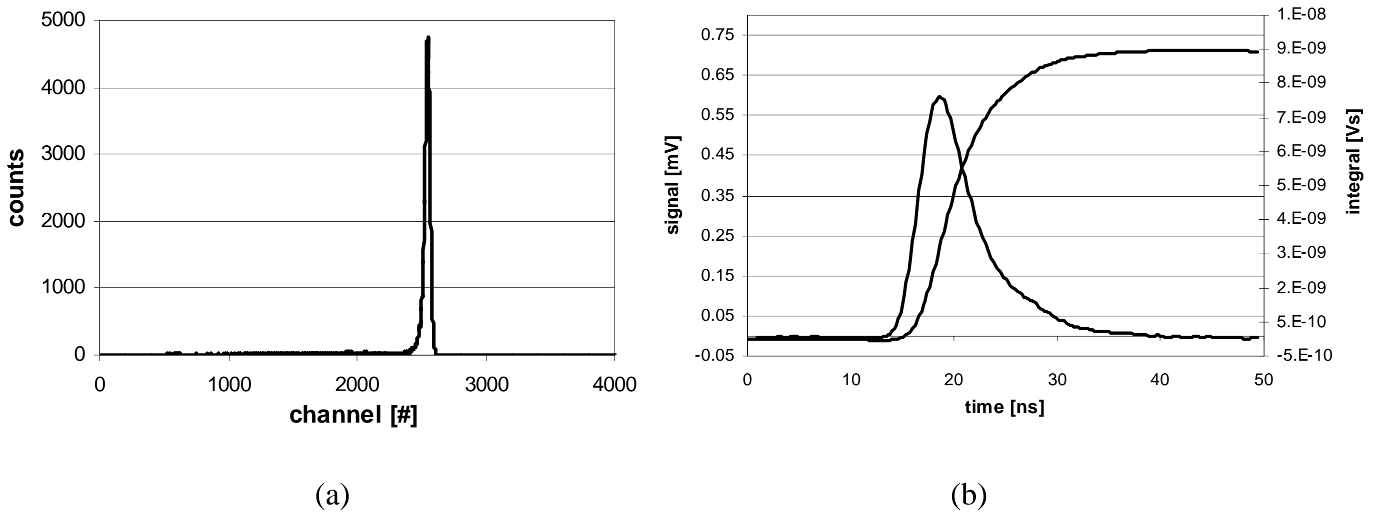

(a) (b)

Fig. 4.14 *Example of (a) energy loss spectrum and (b) signal pulse shape and integral of the signal of an α particle in a fully depleted silicon diode.*

4.3.3 Red light

The red light range in silicon is shown in Fig. 4.15. The absorption coefficient in silicon of red light with a wavelength of 670 ± 50 nm is ≈ 3 10^3 cm^{-1} and almost all the charge is released in less than 7 μm. Therefore, red light produces shallow ionisation and allows a very good electron or hole injection in case of front or rear illumination, respectively. The charge collection behaviours are similar to the charge collection for low range particles, with a maximum ionisation range of 7 μm. For practical purposes this depth is negligible and the charge collection for front illumination of non-irradiated detectors can be expressed by:

$$CC = Q_o, \qquad V \geq 0 \tag{4.27}$$

and, in case of rear illumination by:

$CC = 0$, $\quad V < V_{FD}$ (4.28a)

$CC = Q_o$, $\quad V \geq V_{FD}$. (4.28b)

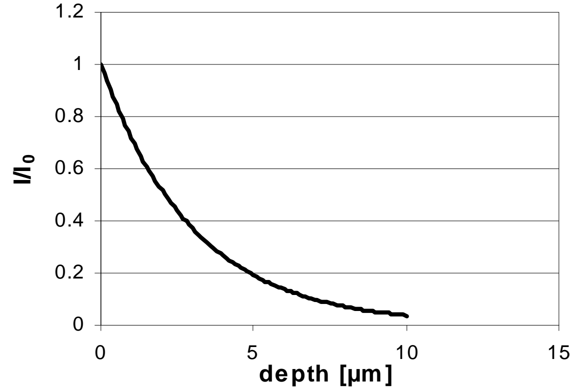

Fig. 4.15 *Ionisation as a function of depth for red (670 nm) light in silicon.*

V_{FD} evaluation

From Fig's. 4.9 and 4.13(b) it is evident that V_{FD} can be evaluated also by CC measurements with MIPs or low range particles. In non-irradiated diodes the estimate is consistent between CC and C-V methods. The limitations of the C-V method applied to irradiated diodes have been discussed. When CC methods are applied to irradiated diodes, some unexpected behaviour appears. The CC versus $V^{1/2}$ measured with β particles are not linear below V_{FD} [2.9] and the charge collection does not saturate at full depletion but continues to increase with a different rate. It is still possible to estimate V_{FD} from the change of the slope of the curve at full depletion, but the error in the estimate increases. Figure 4.16 shows the comparison between the V_{FD} estimate using the C-V and the β charge collection methods.

The estimate of V_{FD} using low range particles injection through the non-junction side fails when applied to heavily irradiated detectors. The reason of the failure is the modification of the electric field, $\boldsymbol{E}$. The distribution of $\boldsymbol{E}$ inside an irradiated diode cannot be represented by a linear shape in the depleted part and a zero electric field in the non-depleted bulk, as it is in non-irradiated detectors. The model of the electric field changes induced by the radiation

presented in Chapter 6 can explain the CC properties for MIP and low range injection for irradiated detectors.

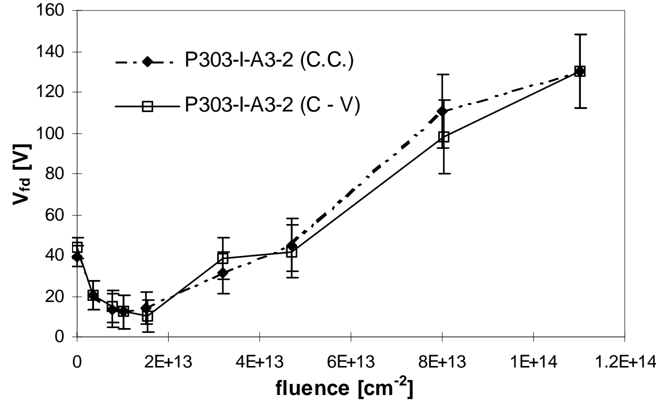

Fig. 4.16 *Comparison between the V_{FD} measurements obtained with the C-V and the β charge collection (C.C.) methods on the same diode irradiated with 24 GeV/c protons.*

4.4 Carrier lifetime measurement

The carrier lifetime is a parameter that accounts for the purity of the silicon crystal. The carrier lifetime is reduced by the trapping due to the presence of energy levels in the forbidden band gap. In particular, levels close to the middle of the band gap are effective in the carrier trapping. Lifetimes fall into two categories: recombination lifetimes (τ_r) and generation lifetimes (τ_g). It has been mentioned that the recombination is the removal of a carrier from the conduction band. It is the dominant effect when excess carriers are injected in the semiconductor (in forward bias mode, or in reverse bias when ionisation takes place). Generation applies when the carrier density is poor, as in a reverse biased semiconductor, and τ_g is the average time to generate an e-h pair. Both processes take place at a deep level in the bandgap and both are reduced while the density of the trapping centres increases.
The radiation introduces deep levels resulting in the reduction of the carrier lifetime. This affects the reverse current and the charge collection efficiency of the detectors. The reverse current is influenced by the generation lifetime (§ 2.2) and the charge collection efficiency is reduced when the recombination lifetime becomes comparable to the collection time.

A method to measure the carrier recombination lifetime is the reverse recovery (RR) method [411, 4.12], illustrated in Fig. 4.17. The diode is biased in a forward mode ($V = V_f$) and a forward current (I_f) flows through the diode. Excess carriers are injected in the quasi-neutral region of the detector. At $t = 0$, the bias is switched to a reverse bias and the current switches to a reverse current (I_r). In a minority carrier devices, the current change is very fast because only a change in the slope of the minority carrier concentration is required.

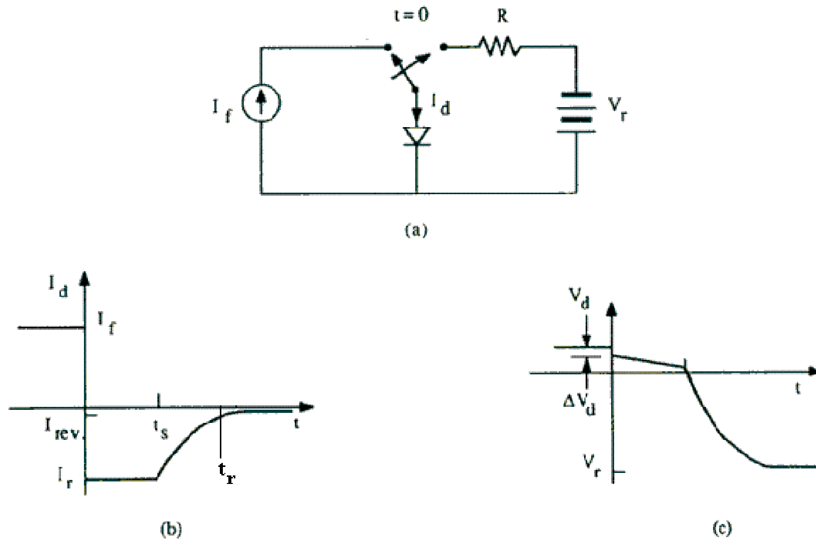

Fig 4.17 *(a) Reverse recovery circuit schematic (b) current and (c) voltage waveforms. At $t = 0$, ΔV_d is due to the drop on the resistance R: $\Delta V_d = RI_r$.*

The diode voltage changes slowly because it is proportional to the logarithm of the excess carrier concentration at the edge of the space charge region. The excess carrier concentration decreases during the reverse current phase: some carriers are swept out of the device from the reverse current and some carriers recombine. The excess minority carrier concentration at the edge of the space charge region is ≈ 0 at $t = t_s$ and the diodes becomes zero biased. For $t > t_s$ the diode voltage approaches the reverse bias voltage and the current reaches the reverse current value. The time t_s is called the storage time. The current curve can be divided in two parts: the constant-storage phase and the recovery phase, when the diode bias goes from zero to the reverse bias voltage. It is related to the lifetime by the expression [4.13]

$$erf\sqrt{\frac{t_s}{\tau_r}} == \left(1 + \frac{I_f}{I_r}\right)^{-1} \tag{4.29}$$

If the measuring system is tuned to have $I_f = I_r$, this relation can be approximated by

$$\tau_r \approx 1.1(t_s + t_r) \qquad (4.30)$$

where t_r is the recovery time (Fig. 4.17). Relation 4.30 can be used to estimate the minority carrier lifetime. Figure 4.18 shows the reverse recovery measurement obtained by a fast oscilloscope for a non irradiated planar diode. The set-up used for the recovery lifetime measurements is shown in Appendix A.

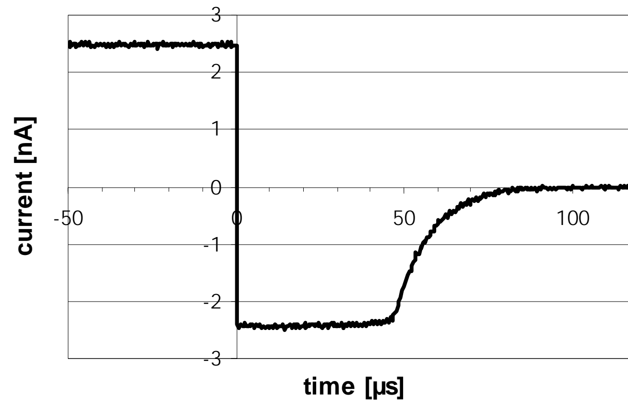

Fig. 4.18 *Reverse recovery signal for a non-irradiated planar diode. The minority carrier lifetime is 70 µs.*

4.4 Irradiation facilities

4.4.1 Proton Irradiation Facility

The proton irradiations have been performed in the PS- east-hall experimental area, feed by the Proton-Synchrotron (PS) accelerator (Fig. 1). The T7 proton beam used has a momentum of 24GeV/c, with negligible momentum spread. The beam is extracted one, two or three times per PS supercycle (14.4 seconds) depending on the beam sharing with other experimental areas. The extracted spill consists of an almost homogeneous burst of protons during ≈400 ms. The underling microstructure of the burst, which frequency is > 1MHz, is negligible for the purpose of irradiation.

The proton beam is defocused in the vertical direction over a length of ≈ 3 cm and it is swept at a constant rate over the crossing time. The resulting beam spot is a quite homogeneous

distribution of 24GeV/c protons over an area 3x2.5 cm^2. The number of particles per spill is about $2 \cdot 10^{11}$, which results in an average proton flux of ≈ $2 \cdot 10^9$ cm^{-2} s^{-1} per spill. Figure 4.19 shows the relative intensity of the beam-spot, obtained by the development of a film exposed to a 5x5 cm^2 aluminium foil activated by ≈ 24 hours exposure to the beam. The 5x5 mm^2 diodes to be irradiated are put in the central region of the beam spot, perpendicularly to the beam direction (z-axis). In this position, the proton flux is the highest and the smooth profile over ≥ 1cm^2 allows a good homogeneity of the irradiation. The diodes are placed inside a box with 5x5cm^2 transverse dimensions and with ≈ 25cm length.

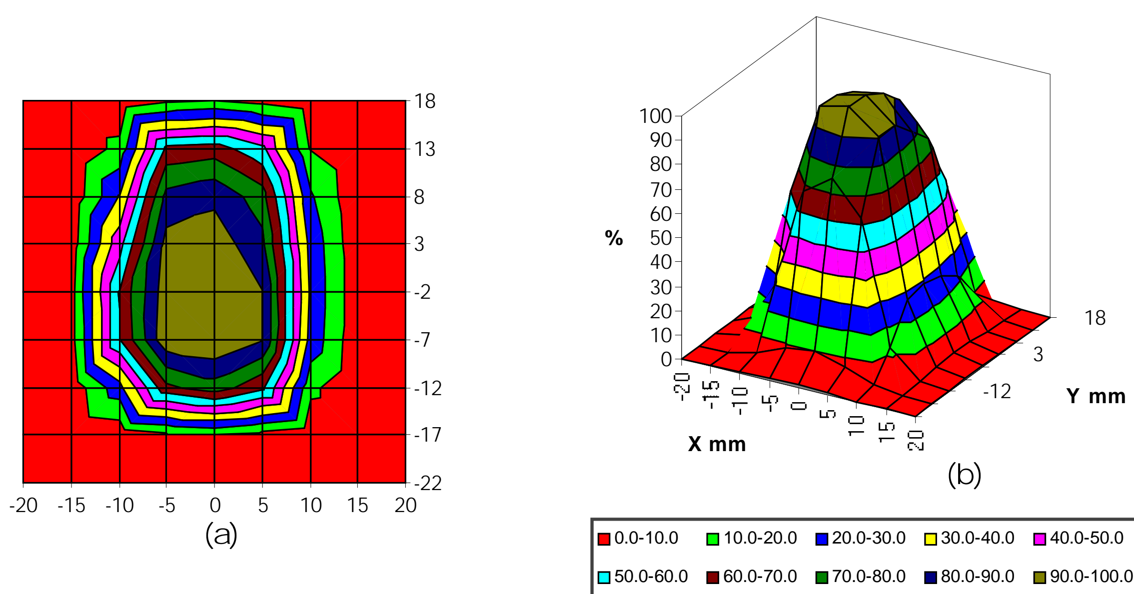

Fig. 4.19 *Beam relative intensity profile (a) front view (b) 3-d view. X is the horizontal co-ordinate and Y is the vertical co-ordinate.*

The detectors are centred with respect to the transverse dimension of the box (holder) by mean of 5x5cm^2 frames, which fit exactly in the holder sides. The number of detectors inside the holder during each irradiation step was limited to ≈ 10 in order to avoid errors in the planned fluence due to multiple scattering effects in the latest detectors in the back of the holder. The holder was aligned at the beginning of the irradiations by means of two glasses positioned at the front and at the back of the box. The superposition of the beam spot on the glasses permits the alignment of the holder in the beam direction with an error < 1mm between the front and

the back. A luminescent screen is aligned to the holder. A CCD camera allows visualising the screen and it is possible to check at any time the position of the beam spot. The holder is moved inside and outside the beam by a remote control motor. The movement to the holder is transmitted through a screw that insures a precise positioning (error < 1mm).
Figure 4.20 shows a sketch of the irradiation holder inside the proton beam.

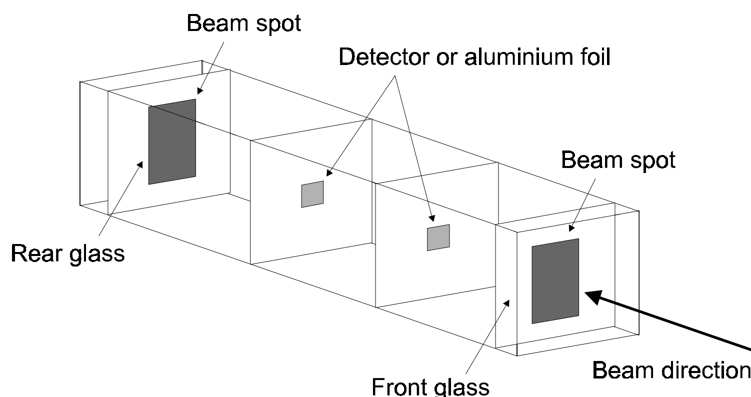

Fig. 4.20 *Sketch of the detector alignment in the proton beam.*

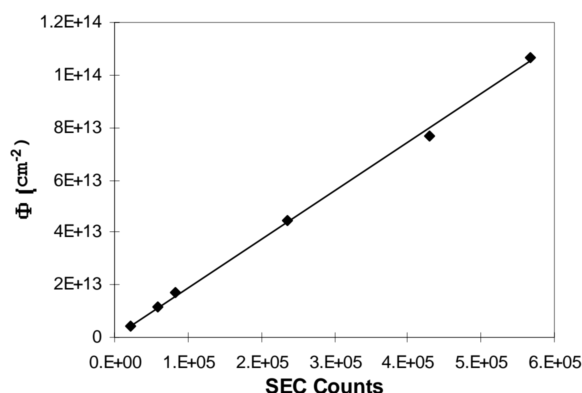

Fig. 4.21 *Fluence (24GeV/c protons) versus Secondary Emission Chamber (SEC) counts.*

The fluence was measured by means of the aluminium-foil activation method [4.12]. An aluminium foil with the same size of the detector was placed close the detector, in the same position with respect to the beam to measure the same average fluence received by the diode.
A secondary emission chamber (SEC), positioned in the beam branch T7, monitors the current of the beam. The SEC provides a sequence of pulses whose number is proportional to the beam intensity. A scaler records the number of pulses. The calibration of the SEC counts to the

fluence measured with aluminium foils allows a good control of the accumulated fluence during the irradiation. Figure 4.21 shows the linearity between the counts of the scaler and the measured fluence. The linearity of the SEC counts to the measured fluence implies negligible error in the detector position inside the beam between two different irradiation runs.

4.4.2 Neutron Irradiation Facility

The neutron irradiations have been performed in the TRIGA Mark II reactor of the Jozef Stefan Institute, Ljubljana, Slovenia. The TRIGA research and training reactor is designed for the radioisotope production and for research operations [4.13]. It can operate at power levels up to > 250 kW. In the fuel elements the zirconium-hydride moderator is homogeneously combined with 20% enriched uranium. These fuel elements exhibit a prompt negative temperature coefficient, which automatically limits the reactor power to a safe level in the event of power excursion. The core is placed in the bottom of a water pool of ≈ 162 cm radius and ≈ 520 cm high. The core is shielded radially by water and by ≈ 160 cm of concrete and vertically by ≈ 400 cm of water. Several beam ports penetrate the concrete shield.

In the core lattice the fuel elements are arranged in six concentric rings. The total number of position in the core is 91. Four irradiation positions are installed in the outer ring plus one in the centre. The temperature of the water in the irradiation region can go up to ≈ 40°C and it is function of the operation power. The maximum neutron flux (in the steady state operation) is > $1\cdot10^{13}$ cm^{-2} s^{-1}. The power regimes used for the irradiation were 2.5, 25 and 250 kW. The corresponding neutron fluxes are 0.026, 0.3 and $0.27\cdot10^{12}$ cm^{-2} s^{-1}, respectively. The operation power was chosen in order to keep the irradiation time ≤ 15 minutes.

The samples to irradiate were placed inside an aluminium cylinder. A tube allows moving the cylinder in the irradiation position inside the reactor core. After the irradiation the samples were lift a few meters and left to cool down the radioactivity before handle them (≈ 15 minutes). The fluence was calculated from reactor specialists using activated gold wires. The neutron flux is relative to fast neutrons. The energy distribution of the fast neutron covers a wide spectrum. The damage factor for this spectrum has been evaluated experimentally and it is $k \approx 7.6$ [4.17].